12-2021

Longitudinal Monitoring of Tumor Response to Immune Checkpoint Inhibitors using Diffuse Optical Spectroscopy

Joel Isaac Rodriguez Troncoso
University of Arkansas, Fayetteville

Longitudinal Monitoring of Tumor Response to Immune Checkpoint Inhibitors using Diffuse Optical Spectroscopy

A thesis submitted in partial fulfillment
of the requirements for the degree of
Master of Science in Biomedical Engineering

by

Joel Rodriguez Troncoso
University of Arkansas
Bachelor of Engineering in Biomedical Engineering, 2019

December 2021
University of Arkansas

This thesis is approved for recommendation to the Graduate Council.

_____
Narasimhan Rajaram, Ph.D.
Thesis Director

_____
Young Hye Song, Ph.D.
Committee Member

_____
Timothy Muldoon, Ph.D.
Committee Member

Abstract

Immune checkpoint drugs have completely changed the way people treat metastatic melanoma and non-small-cell lung cancer. While the impacts of these immunological checkpoints and their suppression on T cell function are well characterized, their consequences on the tumor microenvironment are not.

In a CT26 mouse colorectal cancer model, we employed diffuse reflectance spectroscopy to track in vivo tumor microenvironmental alterations in response to immune checkpoint inhibitors. On three separate days, animals bearing CT26 tumor xenografts were given anti-PD-L1, anti-CTLA-4, a combination of both inhibitors, and isotype control. Within the first 6 days, monotherapy with either anti-PD-L1 or anti-CTLA-4 resulted in a significant increase in tumor vascular oxygenation. The combination of increased oxygenated hemoglobin and decreased deoxygenated hemoglobin caused reoxygenation in anti-CTLA-4-treated tumors, indicating a probable alteration in tumor oxygen consumption following treatment. Reoxygenation was predominantly owing to a rise in oxygenated hemoglobin within a minor change in deoxygenated hemoglobin in anti-PD-L1-treated tumors, indicating a potential increase in tumor perfusion. Except for tumors treated with both inhibitors in combination, none of the other tumor groups demonstrated any reduction in tumor volume. Following therapy, there were no significant changes in tumor oxygenation in the combination treatment group. These results show that diffuse reflectance spectroscopy may detect changes in the tumor microenvironment after immunotherapy and that such non-invasive approaches can be used to predict early tumor response to immune checkpoint inhibitors.

Acknowledgment

First and foremost, I would like to thank Dr. Narasimhan Rajaram. For his unwavering encouragement, mentorship, and support during my undergraduate and graduate years. He provided me with the opportunity to grow and thrive. I will be eternally grateful for his mentorship and constant support through some of the most trying times of my life. It is an understatement to express that this thesis would have not been possible without his aid and constant wisdom.

I would also like to thank Drs. Timothy J. Muldoon, Kyle P. Quinn, and Young Song for their constructive criticism as members of my advisory and thesis committee. In addition, I would like to thank Drs Ishan Barman and Santosh Paidi for their help through our publication.

To my fellow lab members: April Jules, Paola Monterroso Diaz, Lisa Rebello and Jesse Ivers thank you for your collaboration, friendship, and support, and to a former student of our laboratory, Dr. David Lee for playing a significant role in conceptualization the laid-out study.

Very special thanks to Dr. Sina Dadgar, a mentor who has played and important role in my academic and research life, a person who guide me and show constant support, someone I can call a friend.

Lastly, thank you Mom for everything.

Table of Contents

Introduction

Throughout history, three main pillars have been identified for the treatment against cancer: surgery, chemotherapy, and radiation therapy. Currently, with the introduction of immunotherapy, a fourth pillar can be established. Cancer immunotherapy based on targeting immune checkpoint inhibitors (ICIS) has been proven to produce dramatic responses, including responses from patients with metastatic melanoma and non-small-cell lung cancer, but only a small number of patients respond to treatment. Current methods, based on tumor volume changes, fails to account for the immune responds exhibited in tumors treated with different ICI agents. These immunotherapeutic agents may provide responses that are not recorded by the Response Evaluation Criteria in Solid Tumors, such as responses following disease progression. (RECIST) (1-3). Nevertheless, ICIs offers important advantages over traditional treatments such as chemotherapy and radiotherapy (4). Due to a lack of understanding of an immune responsive tumor microenvironment, quantitative data could be used to detect patients who are resistant to treatment. We employed diffuse reflectance spectroscopy (DRS), a non-invasive spectroscopy technique, to identify indicators of immune-checkpoint inhibitor responsiveness in mouse tumor xenografts. As a result, we postulated that immune check point inhibitors cause alterations in the tumor microenvironment that can be detected using optical spectroscopy.

Immune checkpoint inhibitors (ICIs)

ICIs is one of the options for most successful cancer treatment in recent years, with the ability to strengthen the response of T cells against the tumor avoiding the action of molecules capable of inhibiting T cell function. ICIs and immunotherapy in general could be considered as a type of passive immunotherapy, which facilitates and enhances the existing immune response of the body. Currently we have two types of drugs with different mechanisms and places of action: anti CTLA-4 and anti PD / PD-L 1/2.

CTLA-4 is a specialized molecule expressed on T cells during the early stages of their activation in lymphoid organs, known as the priming or priming stage. CTLA-4 interacts with the B7 molecule expressed in the antigen-presenting cell in order to avoid an excessive immune response (unwanted autoimmunity). Thus, CTLA-4 inhibitors, such as ipilimumab, by blocking the CTLA-4 / B7 interaction, deactivate the inhibition signal by increasing the immune response of T cells against the tumor (1-3).

On the other hand, the T lymphocyte stimulated against an antigen expresses on its surface a PD (programmed death receptor) molecule that prevents an over-activation of the immune system. The inactivation signal occurs after the receptor binds to its ligand PD-L1 or PD-L2, usually expressed by dendritic cells or macrophages. However, this mechanism is used by multiple tumors that express large amounts of PD-L1 or PD-L2 on their surface, escaping from the immune system and continuing to proliferate. PD1/2 and PD-L1 / 2 inhibitors, such as atezolizumab, avelumab and durvalumab, act on T cells, being able to stimulate the immune response against tumor cells (1). Patients tolerate anti-CTLA-4 or anti-PD-1 monotherapy quite well, although response rates are poor, with just 13% to 40% of patients showing objective response (2). Patients who get both anti-CTLA-4 and anti-PD-1 therapy had a higher objective response rate, with 55% of patients showing complete response (3). Patients with severe immune-related side events or toxicities, such as dermatitis, colitis, or hepatitis, account for almost the same percentage of patients. In addition, roughly a quarter of individuals who react well to treatment develop secondary resistance. There is strong evidence that changes in the functional and molecular landscape of the tumor microenvironment (TME) between patients account for the considerable inter-patient heterogeneity in responsiveness to ICIs.

Metabolism of an ICI treated tumor

There are certain characteristics of the TME that make it either permissive or restrictive for T cells. Knowing a tumor's functional and molecular profile, as well as how it responds to

ICIs, can help us figure out what elements of the TME allow T cells to assault cancer cells and so enhance response rates. As a result, we will be able to develop more effective therapeutic strategies that can be employed alone or in combination with existing traditional treatments.

T cell metabolism is a fundamental component of the immune response to infection or malignancy and plays an important role in determining immunological response. T cells' metabolic program shifts during an immune response, from oxidative phosphorylation at rest to aerobic glycolysis during clonal proliferation and effector function development (4). Several research have added to our knowledge of the TME's impact on immune cell function (5, 6). Tumors cause a disruption in tissue homeostasis, resulting in a metabolically demanding environment that impacts the stroma and infiltrating immune cells. Aerobic glycolysis, also known as the Warburg effect, refers to the breakdown of glucose to lactate even in the presence of oxygen, which supports cancer cell development. Tumor cells can quickly create the precursors they need for biosynthesis and proliferation thanks to aerobic glycolysis. Although the route is not required for T cell proliferation or survival, it is essential for T cell effector activity (7). These circumstances cause competition between cancer cells and immune cells, increasing the demand for resources, critical metabolites, and oxygen imposed by cancer cell proliferation, resulting in a hostile environment that reduces T cell response (8). When tumor growth outpaces the vasculature's ability to adequately perfuse the microenvironment with oxygen, hypoxia develops, which has a substantial impact on the function of infiltrating T lymphocytes. Tumors treated with anti-PD-1 showed innate anti-PD-1 resistance, which was linked to increased expression of genes involved in mesenchymal transition, cell adhesion, ECM remodeling, and angiogenesis (9). Furthermore, investigations have revealed that PD-L1 expression is linked to glycolysis rate and, as a result, glycolytic enzyme expression. Immune checkpoint blockade, such as PD-L1, causes an increase in extracellular glucose in tumors, which aids in the function of infiltrating T cells and results in a good therapy response (8).

Diffuse reflectance spectroscopy

The ability to noninvasively investigate and measure longitudinal biological changes inside tissue is provided by diffuse reflectance spectroscopy. DRS illuminates tissue using visible to near-infrared light through optical fibers and collects diffusely reflected light after several scattering and absorption events in tissue. Tissue scattering (cells, nuclei, mitochondria, collagen) and absorption (oxygenated and deoxygenated hemoglobin, beta-carotene, melanin) are known to alter with illness progression and are important contributors to our appraisal of disease pathophysiology. DRS can assess volume-averaged vascular oxygenation within sampled tissue using the differential absorption properties of oxygenated and deoxygenated hemoglobin. We discovered that DRS-based sO_2 readings are inversely associated to tumor hypoxia (10). In response to fluctuating oxygen levels, simultaneous and real-time tracking of sO_2 using DRS and tumor pO_2 using oxygen-sensing microelectrodes has showed significant concordance between both measurements (11). We and others have observed different longitudinal changes in tumor vascular oxygenation in response to radiation therapy using DRS's sensitivity to changes in oxygenation, which could potentially aid distinguish between treatment responders and non-responders (12-15). However, no studies have used optical spectroscopy and imaging to track changes in the tumor microenvironment as a result of immune checkpoint inhibitors. The identification of biomarkers of primary and secondary resistance to ICI treatment can be aided by knowledge of such changes.

Thesis Statement

DRS has previously been shown to be capable of detecting changes in tumor oxygenation. Therefore, we hypothesize that optical spectroscopy can identify changes in the tumor microenvironment caused by immune check point inhibitors. The overall purpose of this study was to see how the tumor microenvironment changed over time in response to immune checkpoint inhibitors, which are currently utilized to treat NSCLC and metastatic melanoma. To

produce tumor xenografts in mice, we used the CT26 colorectal cancer cell line. To achieve this goal, we established three specific aims:

1. Generate 4 groups of tumor xenografts for four different types of immune-checkpoint inhibition. The CT26 cell line was chosen for this study because it was used in early pre-clinical investigations to explore ICI responsiveness. Control IgG antibodies, anti-CTLA-4, anti-PD-L1, or a combination of anti-CTLA-4 and anti-PD-L1 antibodies were used to treat tumors.
2. Determine changes in vascular oxygenation (sO_2) and tissue scattering in response to different immune-checkpoint inhibitors and determine the correlation between changes in tumor volume and vascular oxygenation post-treatment and pre-treatment functional parameters
3. Implement a random forest algorithm to test the functional profiles of the generated treatment groups based on the optical parameters acquire through DRS.

Materials and Methods

Cell culture and Tumor xenografts

The American Type Culture Collection (ATCC CRL-2638, Lot Number: 58494154) provided the CT26 colorectal cancer cells, which were passaged according to recognized techniques. For tumor inoculation, cells from the third and fourth passages were employed. Cells were injected into the hind flanks of 6-8-week-old Jackson Laboratories Balb/c mice (n = 33). The mice were kept at the University of Arkansas Central Laboratory Animal Facility, where they were given ad libitum access to food and water and were given 12 hour light/dark cycles. The University of Arkansas' Institutional Animal Care and Use Committee authorized all of the research (IACUC protocols 18066, 20025). Mice were assigned to one of four treatment groups: mouse IgG isotype (control, n = 10), anti-mouse CTLA-4 (CTLA4, n = 8), anti-mouse PD-L1 (PDL1, n = 7) or a combination of CTLA4 and PDL1 (COMB, n = 8). The study's design is depicted in a diagram, Fig. 1a.

Immunotherapy Agents

BioXcell provided the immunotherapy medicines (IgG: MPC-11, CTLA4: UC10-4F10-11, PDL1: 10F.9G2). Mice were given three doses of 100 g anti-CTLA-4, 200 g anti-PD-L1, a combination of the two medicines, or 100 g of IgG control dissolved in 100 l of sterile saline through intraperitoneal injection once tumor sizes reached 80-120 mm3 (16-18). The doses were given on Days 1, 4, and 7, with Day 1 denoting the start of the treatment (Fig. 1a). Three days following their last dose, the animals were euthanized, and tumors were removed and snap-frozen for histology.

Diffuse Reflectance Spectroscopy and quantification of physiological parameters

The portable DRS equipment that was used in this study was previously described in full (10). It is made up of a tungsten halogen lamp (HL-2000, Ocean Optics; Dunedin, FL) for

illumination, a fiber optic spectrometer (Flame, Ocean Optics; Dunedin, FL) for spectrum acquisition, and a fiber optic probe (Fiber Tech Optica, Ontario, Canada). The probe is made up of four source fibers (diameter: 200 m, NA: 0.22) and five detector fibers spaced 2.25 mm from the source fibers' center. On each day, about 10-15 spectra in the wavelength range of 475-650 nm were collected from each tumor. DRS spectra were collected every day for ten days in a row. Prior to ICI administration, spectra were collected on treatment days. We used an empirical lookup table (LUT)-based model (19, 20) developed specifically for this source-detector separation (10) to fit the acquired spectral data and quantify total hemoglobin concentration, oxygenated and deoxygenated hemoglobin, vascular oxygenation, and tissue scattering. Light scattering in tissue was assumed to have a negative power-law dependence on wavelength: $\mu_s'(\lambda) = \mu_s'(\lambda_0).(^{\lambda}/_{\lambda_0})^{-B}$, where λ_0 is a reference wavelength at which light absorption is minimum and is set to 600 nm and μ_s' is the reduced scattering coefficient. The absorption coefficient is calculated as the linear sum of absorption coefficients of individual absorbers, namely oxygenated and deoxygenated hemoglobin, and animal skin: $\mu_a(\lambda) = [\mathrm{Hb}][\alpha\sigma_{\mathrm{HbO_2}}(\lambda) + (1 - \alpha)\sigma_{\mathrm{dHb}}(\lambda)] + [\mathrm{Ml}]\mathrm{mel}(\lambda)$, where [Hb] and [Ml] respectively are total hemoglobin concentration and skin absorption. α is vascular oxygen saturation representing the ratio of oxygenated (HbO_2) to total hemoglobin concentration [Hb]. The extinction coefficients of these absorbers have previously been established. Because we have proven that such effects are minor at wavelengths over 500 nm, the absorption coefficient includes a correction factor for pigment packaging (21). MATLAB was used to analyze the data (MathWorks, Natick, Massachusetts).

Statistical analysis

Optical properties are presented in this manuscript as either absolute values or fold changes. Raw optical properties from Day 1 through 10 were normalized by treatment group to the group mean of the baseline (Day 1 value). Fold change in each optical property is calculated by

dividing the optical property on a given day by the pre-treatment baseline value on Day 1 (Day X/Day 1). A nested, two-way analysis of variance (ANOVA) was implemented to determine statistically significant differences in tissue scattering, hemoglobin concentration and vascular oxygenation across the four treatment groups. Post-hoc Tukey's tests were used to determine statistical significance between specific groups.

Immunohistochemistry

For lipid staining, snap frozen tumors were sectioned on to glass slides and coated with a 0.5 percent Oil Red O in propylene glycol solution and incubated for 45 minutes. After being cleaned and counterstained in Hematoxylin, the slides were dipped in differentiation solution and blue buffer. Before imaging, the slides were mounted with Fluoromount G. A subset of snap frozen tumors was sent to Johns Hopkins University, where they were treated in formalin, embedded in paraffin, and sectioned on glass slides for histopathology and Masson's trichrome staining for collagen visualization. A Nikon fluorescent microscope with a 20X objective was used to image all the slides.

Radom Forrest Analysis

Additionally, to test how the DRS optical phenotype describes from treatment response to ICIs, we employed random forests to test classification of the different treatment groups. The TreeBaggerclass in MATLAB was implemented with 100 trees the code was generate utilizing Dr. Banerjee code and further develop for our study (21). leave-one-mouse-out training strategy was implemented to prevent representation of test mice in the training dataset. The random forests classifiers are trained on the entire optical properties acquired through DRS dataset by excluding all the optical parameters from one mouse at a time and the obtained models are used to test the optical parameters of the left-out mouse. The majority predicted label among all the spectra determines the final predicted label for the test mouse.

Results

Our first objective was to generate four different types of tumor xenografts for four different immune-checkpoint inhibitors treatment. The CT26 cell line was chosen for this study because it had previously been utilized in preclinical studies to investigate ICI responsiveness. The tumor growth curves for each treatment group are shown in figure 1b. While there were no significant differences between groups over the course of the 10-day period, mice receiving a combination of two ICIs (COMB) grew at a slower rate than mice receiving monotherapy (CTLA-4 or PD-L1) or IgG control, this trend is observed in previous studies where the application of a combination treatment consisting of anti-CTLA-4 and anti-PD-L1 had a slow growth rate. Between the groups, there were no significant differences in the mean tumor volume at which therapy was started (Fig. 1c).

Treatment with PD-L1 and CTLA-4 antibodies increases tumor vascular oxygenation

The second objective was to evaluate the link between changes in tumor volume and vascular oxygenation post-treatment and pre-treatment functional characteristics. The fold-changes in vascular oxygenation (top row) and total hemoglobin concentration (bottom row) for the three treatment groups – PD-L1, CTLA-4, and COMB – during a 10-day period are shown in Figure 2. Each plot includes data from the control IgG group for a one-to-one comparison with each treatment group. The IgG group mean sO_2 declined gradually throughout the 10-day period, reaching 0.5x of the Day 1 baseline by Day 10, with a corresponding increase in total hemoglobin concentration. In the first six days, treatment with αPD-L1 or αCTLA-4 alone resulted in an increase in vascular oxygenation. αCTLA-4 group mean f-sO2 increased significantly (1.5X baseline sO_2) 24 hours after the first dosage. The largest fold-change in sO2 was on day 5, 24 hours after the second dose, and decreased to pre-treatment levels by day 10.

On any given day, however, there were no significant changes between the IgG and αCTLA-4 groups. In addition, there were no significant differences in cHb from baseline. The mean f-sO_2

in the αPD-L1 group increased gradually, with a peak value of fold-change at Day 6 and a significant difference between the αPD-L1 and IgG control groups (p 0.001). On Day 10, the fold-change in cHb was much higher than the fold-change on the previous five days. In comparison to the αPD-L1 and αCTLA-4 groups, mean sO_2 and cHb fluctuated very little over time.

We looked at the trends in oxygenated (HbO_2) and deoxygenated (Hb) Hb to see what was causing the variations in sO2 and cHb in each of the treatment groups (dHb). The IgG group's gradual decline can be explained almost completely to a considerable increase in dHb over time, implying an increase in oxygen demand and consumption as tumors grow larger (Fig. 3). We discovered that the substantial rise in sO_2 24 hours after the initial dosage in αCTLA-4 - treated mice was related to a decrease in dHb and a corresponding increase in HbO_2. There was a 28% decrease in mean dHb and a 25% increase in mean HbO_2 in particular. This trend of elevated HbO_2 and decreased dHb continued for the next 4 days until Day 6. Beginning Day 7, we observe an increase in dHb and a corresponding decrease in HbO_2 that contributes to the decrease in sO_2. On the other hand, the increase in sO_2 in the tumors treated with PD-L1 were driven by change in HbO_2 only, with very minor changes in dHb. Finally, both HbO_2 and dHb in the COMB group showed little to no variation over the 10-day period, which explains the lack of change in mean sO_2 of the COMB group.

Changes in Vascular Oxygenation is negatively correlated to baseline SO_2

Following data processing, we looked at whether changes in tumor oxygenation after therapy were influenced by pre-treatment, baseline vascular oxygenation in each group. Tumor reoxygenation was observed to be moderately to substantially adversely linked with baseline vascular oxygenation 24 hours after each dosage of ICI treatment (Fig. 4). In the αPD-L1 group, there was a very weak association between fold-change in sO_2 on Day 2 and baseline sO_2, although this correlation grew stronger by Day 5 ($r = -0.55$) and was statistically significant by

Day 8 (r = -0.75, p = 0.02). Furthermore, on Day 2 (r = -0.7, p = 0.05), we found a statistically significant negative correlation in the combined therapy group (r = -0.7, p = 0.05), and this negative correlation was high across all three evaluation time points (r = -0.66 to -0.73). Similarly, we wanted to test whether changes in tumor volume in response to ICIs are correlated with pre-treatment vascular oxygenation or Hb. In figure 5, correlation plots for vascular oxygenation and total hemoglobin content for αCTLA-4, PD-L1 and COMB against the percent change in tumor volume on day 9. Anatomical changes in tumor volume in response to ICIs are not correlated with pre-treatment vascular oxygenation or cHb.

PD-L1 antibody treatment causes significant changes in tissue scattering

Figure 6 presents a comparison in scattering content between the control group IgG against the treatment groups αCTLA-4, αPD-L1 and COMB. Figure 6C, scattering content across the three dosages for the IgG and COMB groups showed no significant changes. αCTLA-4 group denotes a slight increase in scattering content after the first dosage of treatment (figure 4A). This upward trend is carried up to the third treatment dosage where it does show a decrease in the scattering content. On the other hand, the αPD-L1 treatment group shows significant difference on nine consecutive days in comparison to day one of DRS (figure 6B). The main source of scattering in diffuse reflectance spectroscopy comes from collagen content within the tissue of interest. These results potentially showed a difference in collagen content in the αPD-L1 group in comparison to αCTLA-4 and COMB.

Classification of optical parameters through Random Forrest Analysis allows prediction of ICI's

Our third objective consisted of using the optical parameters obtained from DRS in a random forest algorithm to test classification of the ICI treatment groups. Because spectrum datasets from CT26 tumors treated with two different immune checkpoint inhibitors, αCTLA-4 and αPD-L1, and a combination treatment were available, we were able to use random forest

classification analysis to test the functional parameters. In table 1, we observed predicted labels against the true labels of the tested optical parameters. The IgG group was correctly classified with 7 out of 8 animals categorized as being part of the control IgG group. Similarly, the αPD-L1 treatment group denoted a 78% positive classification where 7 out of 9 animals were categorized correctly, while the remaining mice were categorized in the COMB group. The αCTLA-4 had a success greater than 50%, where 6 out of the 9 animals were classified in their true labels. However, the three remaining were categorized in the αPD-L1 and the COMB group. From the tested, the random forest algorithm showed difficulties classifying the COMB group. Only 36% percent of the animals, meaning 3 out of the 8 mice, were classified correctly. The remaining mice in the COMB group were categorized as follow, one in the IgG group, 3 out of the 8 in the αPD-L1 treatment group, and the remaining mouse in the αCTLA-4 group. Figure 7 shows representative hematoxylin and eosin (H&E)-stained pictures for each group and Masson's Trichrome images. While tumor volume did not change significantly between treatment groups at the time of excision, the animals in the combination treatment group (COMB) showed higher degrees of necrosis than the isotype control and monotherapy groups (Fig. 7G). Similarly, it is noted that the αPD-L1 has higher levels of collagen staining represented by the blue hue in figure 7F.

Discussion

Metabolic reprogramming of tumor cells and the tumor microenvironment has emerged as a critical component in controlling immune cell infiltration and ICI response (22, 23). Increased mitochondrial oxidative metabolism in cancer cells, which leads to intratumoral hypoxia and T cell exhaustion due to a lack of oxygen supply, inhibits T cell proliferation and, thus, response to ICIs, in the same way that tumor hypoxia causes poor clinical outcomes in tumors treated with radiation therapy (24-27). Tumor hypoxia is a metabolically restricted environment that increases the stimulation of immunosuppressive regulatory T cells, reduces T cell receptor signaling, inhibits effector T cell function, and lowers cytokine output (28, 29). Several research have investigated the ability of noninvasive optical imaging and spectroscopy to track changes in tumor oxygenation after traditional cancer treatments like radiation and chemotherapy (12-15, 30-32). Using diffuse reflectance spectroscopy, we offer the first assessment of functional alterations within the tumor microenvironment in response to ICIs. We employed CT26 colorectal cancer cells to produce tumor xenografts in mice and measured changes in tumor vascular oxygenation, hemoglobin content, and tissue scattering over time after treating these tumors with either single ICIs or a combination of ICIs.

While there were no significant variations in tumor volume between the treatment groups at the time of excision, the animals treated with PD-L1 and CTLA-4 in combination had a lower tumor volume than the other groups. Furthermore, when compared to the isotype control and monotherapy groups, these tumors had higher levels of necrosis (Fig. 7). While monotherapy and combination therapy normally produce responses in roughly 20% and 50% of tumors, respectively, the lack of meaningful improvement seen here is most likely attributable to the research design. We waited for palpable tumor masses (about 80-150 mm3) to develop to ensure we could perform baseline optical spectroscopy on tumors prior to treatment, unlike

most ICI studies, which involve cancer cell inoculations followed by ICI treatment in a short period of time (within 2-3 days).

In tumors treated with anti-CTLA-4 and anti-PD-L1 monotherapy, we discovered a significant increase in vascular oxygenation or reoxygenation. The cause of the alteration, however, was different in both groups. While an increase in oxygenated hemoglobin and a corresponding drop in deoxygenated hemoglobin drove reoxygenation in anti-CTLA-4-treated tumors, anti-PD-L1-treated tumors only demonstrated an increase in oxygenated hemoglobin and no change in deoxygenated hemoglobin. These data show that inhibiting immunological checkpoints promotes vascular oxygenation, implying that tumor hypoxia is reduced. Different mechanisms are at work to induce these changes, according to data from oxygenated and deoxygenated hemoglobin. Variations in supply or demand could cause changes in vascular oxygenation. Cancer cell death and decreased oxygen consumption by tumor cells cause the vasculature to use less oxygen, resulting in a drop in deoxygenated hemoglobin, an increase in oxygenated hemoglobin, and, as a result, an increase in vascular oxygenation. Increased perfusion in response to microenvironmental perturbations, on the other hand, will result in an increase in oxygenated hemoglobin, which will lead to an increase in vascular oxygenation. Data from isotype-treated tumors demonstrate a progressive decrease in vascular oxygenation (increased hypoxia) caused by a rise in deoxygenated hemoglobin, indicating increasing oxygen demand. The formation of new tumor vasculature to supply the proliferating cancer cells in these untreated tumors is illustrated by the equivalent increase in total hemoglobin content. Tumors treated with anti-PD-L1 showed an increase in oxygenated hemoglobin with no change in deoxygenated hemoglobin, indicating a likely increase in perfusion. Further studies on excised tumors at specific timepoints of interest in this study will be necessary to evaluate whether these perfusion-related changes were associated with or due to increased immune cell infiltration. In the first 5 days following treatment with anti-CTLA-4, the increased sO2 was due

to a combination of increased HbO2 and decreased dHb. Since this did not lead to an appreciable decrease in total hemoglobin concentration, these data indicate that these changes were likely due to decreased oxygen consumption by the tumor cells. Furthermore, based on our random forest classification these functional changes can be potentially used to categorize treatment response to ICI's. We know that the use of checkpoint inhibitors, specifically anti-PD-L1, have been shown to decrease tumor glycolysis and increase the availability of glucose for effector T cells in the tumor microenvironment (8,9). In addition, elevated mitochondrial oxidative metabolism in tumor cells has been shown to decrease the efficacy of anti-PD-1 therapy in pre-clinical and clinical studies (26). By introducing a non-invasive technique functional profile can be acquire to further study patient's reaction to treatment.

Anti-CTLA-4 and anti-PD-L1 therapy resulted in a considerable increase in collagen I deposition in an orthotopic model of CT26 tumors, according to previous research (33). However, in the combined therapy group, we found no significant alterations in tissue scattering, which includes collagen as one of its origins. The anti-PD-L1 therapy group had a slight but substantial increase in tissue scattering compared to the control group. While the increase in tissue dispersion and perfusion in response to anti-PD-L1 treatment was minor, it warrants additional exploration into the possibility of immune cell infiltration. While collagen, cells, nuclei, and mitochondria are thought to be important contributors to overall tissue scattering, little is known about the contributions of immune cell infiltration to tissue scattering and if they are big enough to cause major changes. Furthermore, necrotic tissue has been linked to an increase in optical scattering. When comparing the monotherapy and isotype control groups, histological analysis of the tumor groups revealed that the combination treatment group had higher degrees of necrosis. The longitudinal variations in optical scattering, however, do not reflect this.

While earlier research has looked at the negative effects of hypoxia, acidification, and decreased glucose availability on immune cells and immune checkpoint inhibitor activity, there

has been little research into how immune checkpoint inhibitors affect tumor metabolism. Other studies addressing changes in tumor oxygenation following therapy with immune checkpoint inhibitors were not found in the literature. Our findings show a significant increase in tumor oxygenation after ICI treatment, and that the source of reoxygenation is likely depending on the ICI type. The magnitude of reoxygenation was inversely proportional to baseline sO2. However, to determine the contributions of immune cells to the functional changes shown here, these findings must be examined in immuno-compromised animals lacking mature T cells.

References

1. Villadolid J, Amin A. Immune checkpoint inhibitors in clinical practice: update on management of immune-related toxicities. Transl Lung Cancer Res. 2015;4(5):560-75. doi: 10.3978/j.issn.2218-6751.2015.06.06. PubMed PMID: 26629425; PMCID: PMC4630514.

2. Gibney GT, Weiner LM, Atkins MB. Predictive biomarkers for checkpoint inhibitor-based immunotherapy. The Lancet Oncology. 2016;17(12):e542-e51.

3. Larkin J, Chiarion-Sileni V, Gonzalez R, Grob JJ, Cowey CL, Lao CD, Schadendorf D, Dummer R, Smylie M, Rutkowski P. Combined nivolumab and ipilimumab or monotherapy in untreated melanoma. New England journal of medicine. 2015;373(1):23-34.

4. Pearce EL, Poffenberger MC, Chang C-H, Jones RG. Fueling Immunity: Insights into Metabolism and Lymphocyte Function. Science. 2013;342(6155):1242454. doi: 10.1126/science.1242454.

5. Pearce EL, Pearce EJ. Metabolic pathways in immune cell activation and quiescence. Immunity. 2013;38(4):633-43.

6. Buck MD, Sowell RT, Kaech SM, Pearce EL. Metabolic instruction of immunity. Cell. 2017;169(4):570-86.

7. Chang C-H, Curtis Jonathan D, Maggi Leonard B, Faubert B, Villarino Alejandro V, O'Sullivan D, Huang Stanley C-C, van der Windt Gerritje JW, Blagih J, Qiu J, Weber Jason D, Pearce Edward J, Jones Russell G, Pearce Erika L. Posttranscriptional Control of T Cell Effector Function by Aerobic Glycolysis. Cell. 2013;153(6):1239-51.

8. Chang C-H, Qiu J, O'Sullivan D, Buck Michael D, Noguchi T, Curtis Jonathan D, Chen Q, Gindin M, Gubin Matthew M, van der Windt Gerritje JW, Tonc E, Schreiber Robert D, Pearce Edward J, Pearce Erika L. Metabolic Competition in the Tumor Microenvironment Is a Driver of Cancer Progression. Cell. 2015;162(6):1229-41.

9. Hugo W, Zaretsky JM, Sun L, Song C, Moreno BH, Hu-Lieskovan S, Berent-Maoz B, Pang J, Chmielowski B, Cherry G. Genomic and transcriptomic features of response to anti-PD-1 therapy in metastatic melanoma. Cell. 2016;165(1):35-44.

10. Dadgar S, Troncoso JR, Rajaram N. Optical spectroscopic sensing of tumor hypoxia. Journal of Biomedical Optics. 2018;23(6). doi: 10.1117/1.JBO.23.6.067001. PubMed PMID: WOS:000439236300020.

11. Palmer GM, Viola RJ, Schroeder T, Yarmolenko PS, Dewhirst MW, Ramanujam N. Quantitative diffuse reflectance and fluorescence spectroscopy: tool to monitor tumor physiology in vivo. Journal of Biomedical Optics. 2009;14:024010.

12. Dadgar S, Troncoso JR, Siegel ER, Curry NM, Griffin RJ, Dings RPM, Rajaram N. Spectroscopic investigation of radiation-induced reoxygenation in radiation-resistant tumors. Neoplasia. 2021;23(1):49-57.

13. Diaz PM, Jenkins SV, Alhallak K, Semeniak D, Griffin RJ, Dings RPM, Rajaram N. Quantitative diffuse reflectance spectroscopy of short-term changes in tumor oxygenation after

radiation in a matched model of radiation resistance. Biomedical Optics Express. 2018;9(8):3794-804. doi: 10.1364/BOE.9.003794.

14. Hu F, Vishwanath K, Salama JK, Erkanli A, Peterson B, Oleson JR, Lee WT, Brizel DM, Ramanujam N, Dewhirst MW. Oxygen and perfusion kinetics in response to fractionated radiotherapy in FaDu head and neck cancer xenografts are related to treatment outcome. International Journal of Radiation Oncology*Biology*Physics. 2016;96(2):462-9. doi.

15. Vishwanath K, Klein D, Chang K, Schroeder T, Dewhirst MW, Ramanujam N. Quantitative optical spectroscopy can identify long-term local tumor control in irradiated murine head and neck xenografts. Journal of Biomedical Optics. 2009;14(5):054051--4. doi: 10.1117/1.3251013.

16. Duraiswamy J, Kaluza KM, Freeman GJ, Coukos G. Dual Blockade of PD-1 and CTLA-4 Combined with Tumor Vaccine Effectively Restores T-Cell Rejection Function in Tumors. Cancer Research. 2013;73(12):3591-603. doi: 10.1158/0008-5472.Can-12-4100.

17. Selby MJ, Engelhardt JJ, Johnston RJ, Lu L-S, Han M, Thudium K, Yao D, Quigley M, Valle J, Wang C, Chen B, Cardarelli PM, Blanset D, Korman AJ. Preclinical Development of Ipilimumab and Nivolumab Combination Immunotherapy: Mouse Tumor Models, In Vitro Functional Studies, and Cynomolgus Macaque Toxicology. PLOS ONE. 2016;11(9):e0161779. doi: 10.1371/journal.pone.0161779.

18. Chang C-H, Qiu J, O'Sullivan D, Buck MD, Noguchi T, Curtis JD, Chen Q, Gindin M, Gubin MM, Van Der Windt GJ. Metabolic competition in the tumor microenvironment is a driver of cancer progression. Cell. 2015;162(6):1229-41.

19. Nichols BS, Rajaram N, Tunnell JW. Performance of a lookup table-based approach for measuring tissue optical properties with diffuse optical spectroscopy. Journal of Biomedical Optics. 2012;17(5). doi: 10.1117/1.JBO.17.5.057001. PubMed PMID: WOS:000305579600025.

20. Rajaram N, Nguyen T, Tunnell J. Lookup table-based inverse model for determining optical properties of turbid media. Journal of Biomedical Optics. 2008;13(5). doi: 10.1117/1.2981797. PubMed PMID: WOS:000261764900001.

21. Dr. Soumya Banerjee (2021). Simple example code and generic function for random forests, MATLAB Central File Exchange. Retrieved August 10, 2021.

22. Rajaram N, Gopal A, Zhang X, Tunnell J. Experimental Validation of the Effects of Microvasculature Pigment Packaging on In Vivo Diffuse Reflectance Spectroscopy. Lasers in Surgery and Medicine. 2010;42(7):680-8. doi: 10.1002/lsm.20933. PubMed PMID: WOS:000281492300011.

23. Le Bourgeois T SL, Aksoylar HI, Daneshmandi S, Seth P, Patsoukis N, Boussiotis VA. Targeting T Cell Metabolism for Improvement of Cancer Immunotherapy. Frontiers in Oncology. 2018;8:237.

24. Mushtaq MU PA, Pagenkopf A, Flietner E, Morrow Z, Chaudhary SG, Asimakopoulos F. Tumor matrix remodeling and novel immunotherapies: the promise of matrix-derived immune biomarkers. Journal for Immunotherapy of Cancer. 2018;6(1):65.

25. Brizel D, Sibley G, Prosnitz L, Scher R, Dewhirst M. Tumor hypoxia adversely affects the prognosis of carcinoma of the head and neck. International Journal of Radiation Oncology* Biology* Physics. 1997;38(2):285-9.

26. Nordsmark M, Bentzen S, Rudat V, Brizel D, Lartigau E, Stadler P, Becker A, Adam M, Molls M, Dunst J. Prognostic value of tumor oxygenation in 397 head and neck tumors after primary radiation therapy. An international multi-center study. Radiotherapy and Oncology. 2005;77(1):18-24.

27. Najjar YG, Menk AV, Sander C, Rao U, Karunamurthy A, Bhatia R, Zhai S, Kirkwood JM, Delgoffe GM. Tumor cell oxidative metabolism as a barrier to PD-1 blockade immunotherapy in melanoma. JCI Insight. 2019;4(5). doi: 10.1172/jci.insight.124989.

28. Scharping NE, Menk AV, Whetstone RD, Zeng X, Delgoffe GM. Efficacy of PD-1 Blockade Is Potentiated by Metformin-Induced Reduction of Tumor Hypoxia. Cancer Immunology Research. 2017;5(1):9-16. doi: 10.1158/2326-6066.cir-16-0103.

29. Rivadeneira DB, Delgoffe GM. Antitumor T-cell reconditioning: improving metabolic fitness for optimal cancer immunotherapy. Clinical cancer research. 2018;24(11):2473-81.

30. Neumann AK, Yang J, Biju MP, Joseph SK, Johnson RS, Haase VH, Freedman BD, Turka LA. Hypoxia inducible factor 1α regulates T cell receptor signal transduction. Proceedings of the National Academy of Sciences of the United States of America. 2005;102(47):17071-6. doi: 10.1073/pnas.0506070102.

31. Sunar U, Quon H, Durduran T, Zhang J, Du J, Zhou C, Yu G, Choe R, Kilger A, Lustig R, Loevner L, Nioka S, Chance B, Yodh AG. Noninvasive diffuse optical measurement of blood flow and blood oxygenation for monitoring radiation therapy in patients with head and neck tumors: a pilot study. Journal of Biomedical Optics. 2006;11(6):064021--13. doi: 10.1117/1.2397548.

32. Tabassum S, Tank A, Wang F, Karrobi K, Vergato C, Bigio IJ, Waxman DJ, Roblyer D. Optical scattering as an early marker of apoptosis during chemotherapy and antiangiogenic therapy in murine models of prostate and breast cancer. Neoplasia. 2021;23(3):294-303.

33. Roblyer D, Ueda S, Cerussi A, Tanamai W, Durkin A, Mehta R, Hsiang D, Butler JA, McLaren C, Chen WP. Optical imaging of breast cancer oxyhemoglobin flare correlates with neoadjuvant chemotherapy response one day after starting treatment. Proceedings of the National Academy of Sciences. 2011;108(35):14626-31.

34. Fiegle E, Doleschel D, Koletnik S, Rix A, Weiskirchen R, Borkham-Kamphorst E, Kiessling F, Lederle W. Dual CTLA-4 and PD-L1 Blockade Inhibits Tumor Growth and Liver Metastasis in a Highly Aggressive Orthotopic Mouse Model of Colon Cancer. Neoplasia. 2019;21(9):932-44. doi: https://doi.org/10.1016/j.neo.2019.07.006.

35. Troncoso JR**,** Diaz PM, Lee D, Quick C, Rajaram N, *Longitudinal monitoring of tumor response to immune checkpoint inhibitors using noninvasive diffuse reflectance spectroscopy*. Biomedical optics express 12(7):3982, 2021.

Tables and Figures

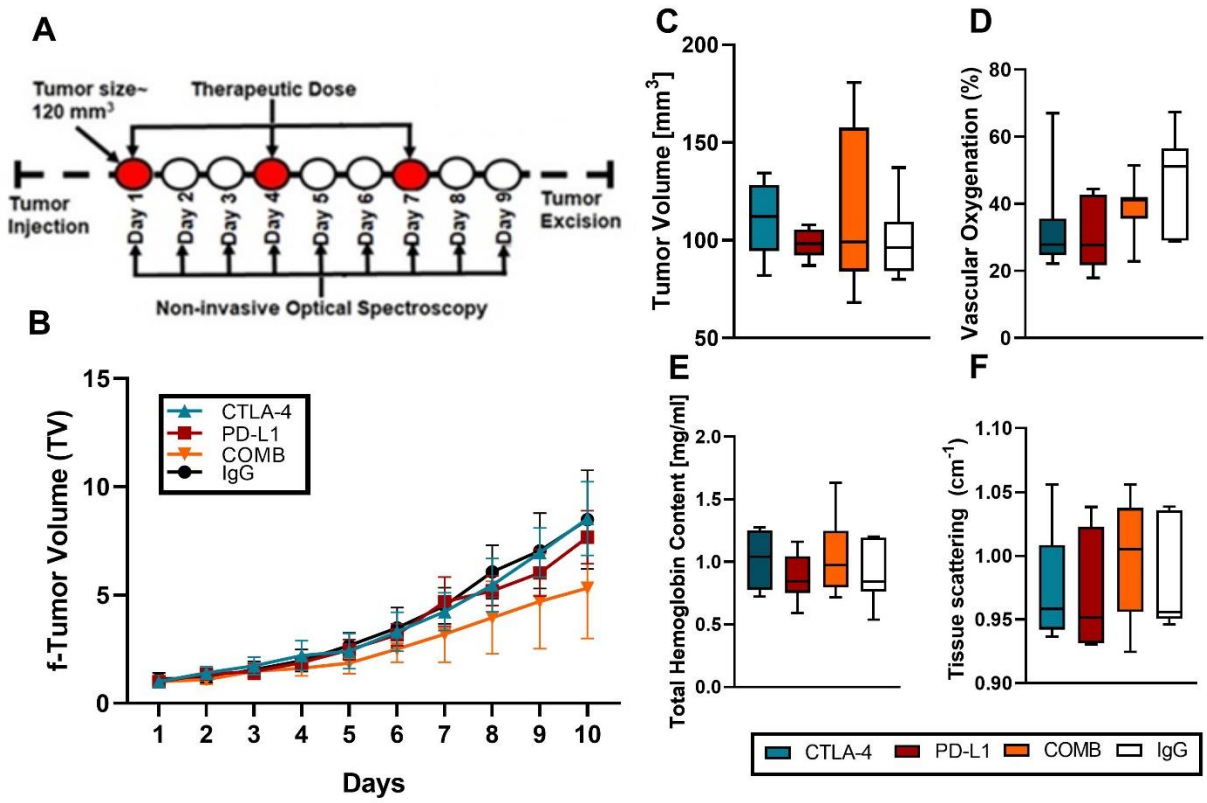

Figure 1. Study design for immune check-point inhibitor treatment. (**A)** Timeline for the schedule of immune-checkpoint inhibitors injection and spectroscopic measurement. The red circles indicate treatment injection for the different groups. As indicated by the arrows, DRS was performed for 9 consecutive days. On days of treatment, DRS spectra were collected immediately after ICI injection. Comparison of the fold change of tumor growth for the treatment groups, IgG, CTLA-4, PD-L1 and COMB **(B)** and baseline values comparison of tumor volume, vascular oxygenation, total hemoglobin content and tissue scattering **(C, D, E, F,** respectively**).**

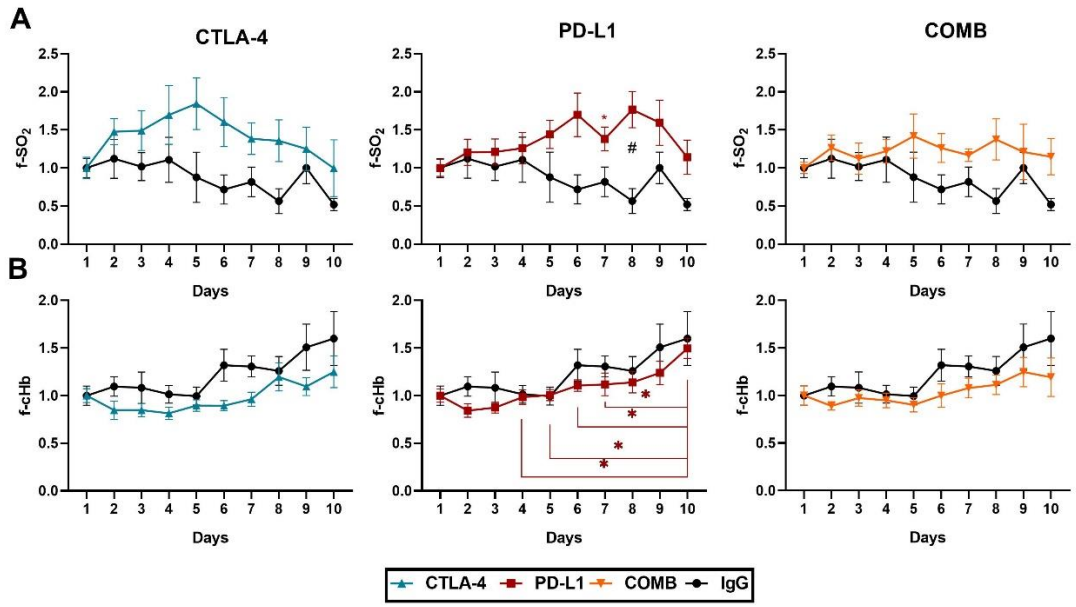

Figure 2. (A) Linear plots for percent change in vascular oxygenation for CTLA-4, PD-L1 and COMB against the control group IgG across the 10 days of DRS. **(B)** Percent change in total hemoglobin content for the four treatment groups across 10 days of spectroscopy. Data are presented as group mean (line) ±SEM (represented by error bars). Significant differences among treatments in specific days are illustrated with black pounds (#) while significant differences of specific days within groups are represented by asterisk of their respective color indicating a statistical significance at $p < 0.05$.

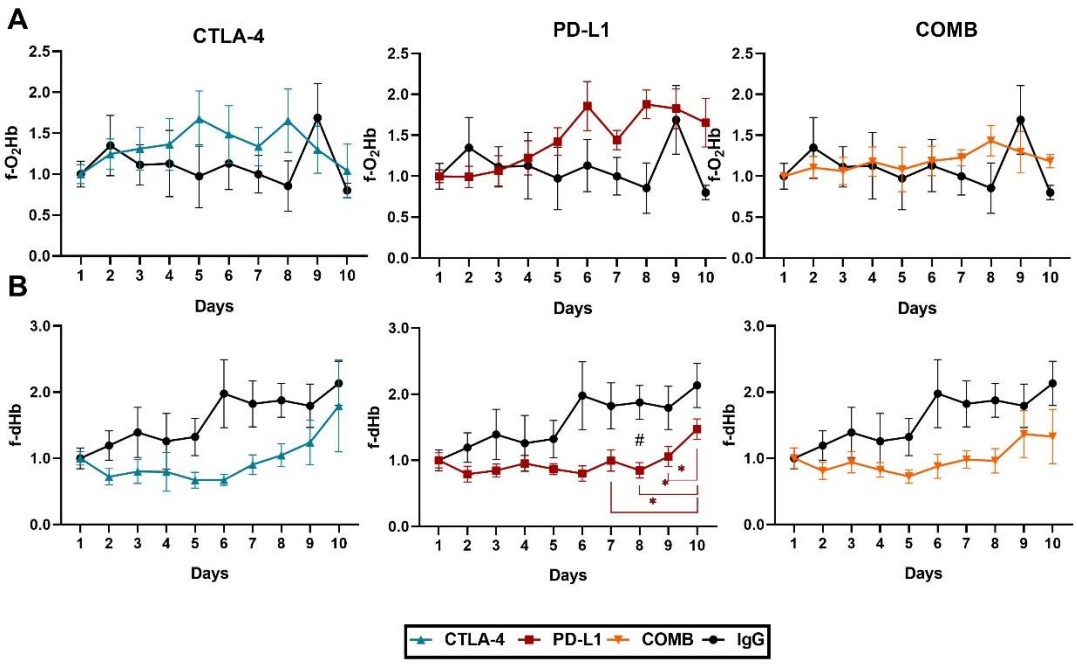

Figure 3 (A) Linear plots for percent change in oxygenated hemoglobin for CTLA-4, PD-L1 and COMB against the control group IgG across the 10 days of DRS. **(B)** Percent change in deoxygenated hemoglobin content for the four treatment groups across 10 days of spectroscopy. Data are presented as group mean (line) ±SEM (represented by error bars). Significant differences among treatments in specific days are illustrated with black pounds (#) while significant differences of specific days within groups are represented by asterisk of their respective color indicating a statistical significance at $p < 0.05$.

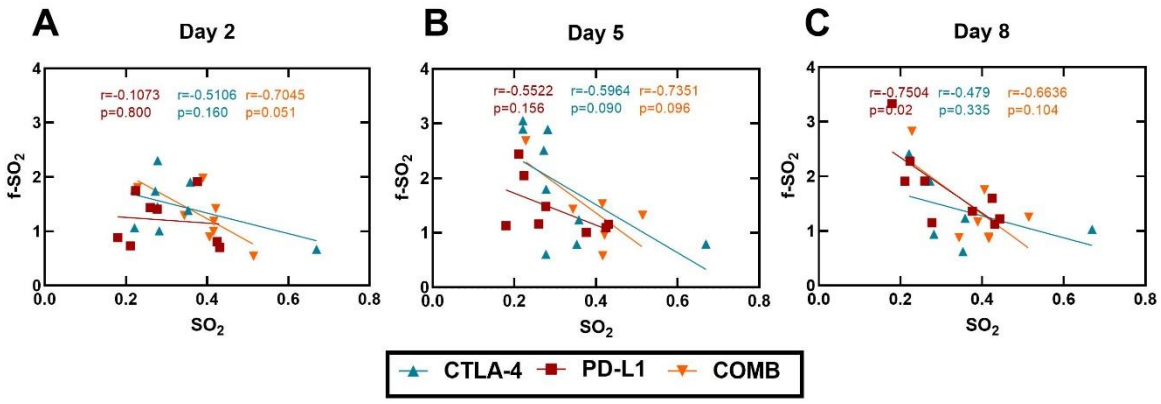

Figure 4 Scatter plots representing the relationship between fold changes in SO_2 and base line vascular oxygenation for the groups CTLA-4, PD-L1 and COMB 24 hours the respective dosage, day 2 **(A)**, day 5 **(B)**, and day 8 **(C)**. Linear regressions for the respective groups are represented by the solid lines, *r* and *p* values are shown for old the groups with a significant difference at $p < 0.05$.

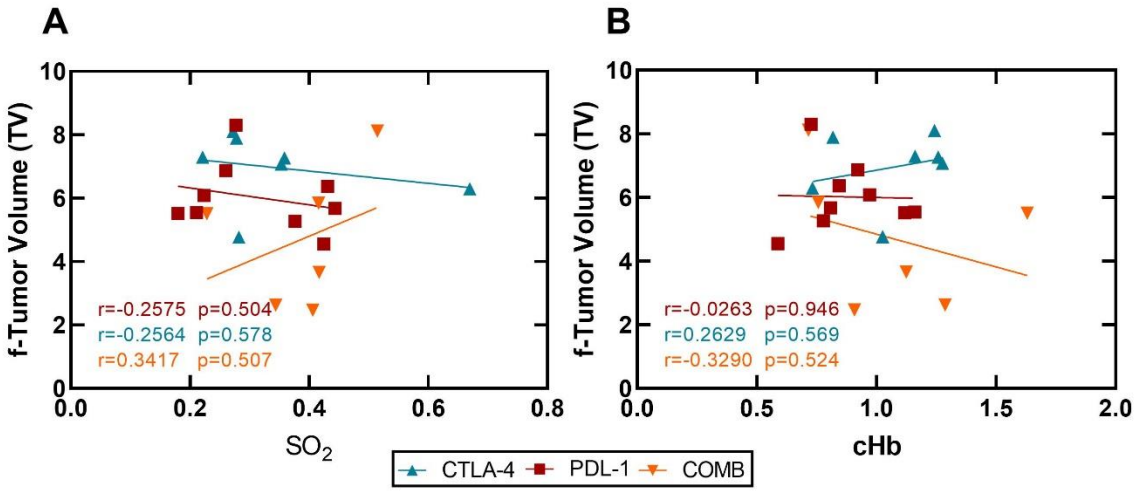

Figure 5. Scatter plots representing the relationship between fold changes in tumor volume DRS-based measures of (A) sO2, (B) cHb. Linear regressions for the respective groups are represented by the solid lines, r and p values are shown for old the groups with a significant difference at $p < 0.05$.

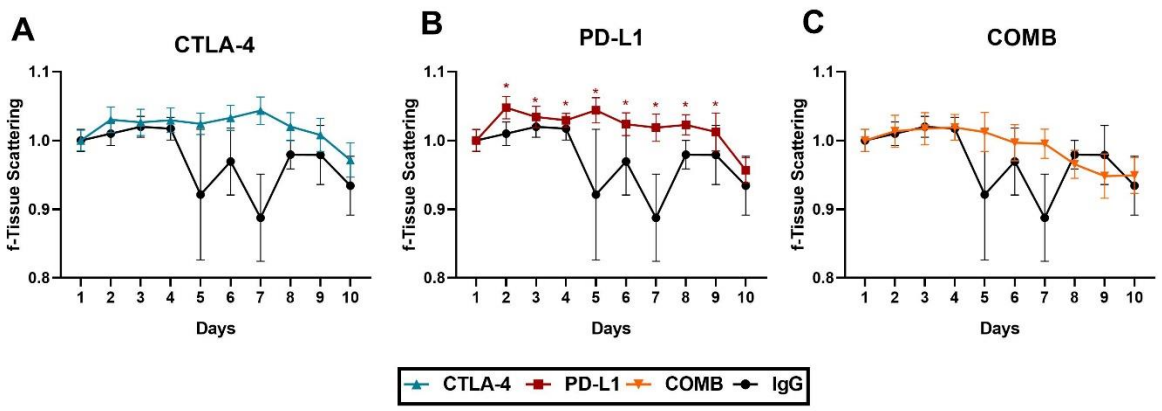

Figure 6 Linear plots for scattering content for CTLA-4, PD-L1, and COMB against the control group IgG **(A, B, and C** respectively**)** across 10 days of spectroscopy. Data are presented as group mean (line) ±SEM (represented by error bars). Significant differences of specific days within groups are represented by asterisk of their respective color indicating a statistical significance at $p < 0.05$.

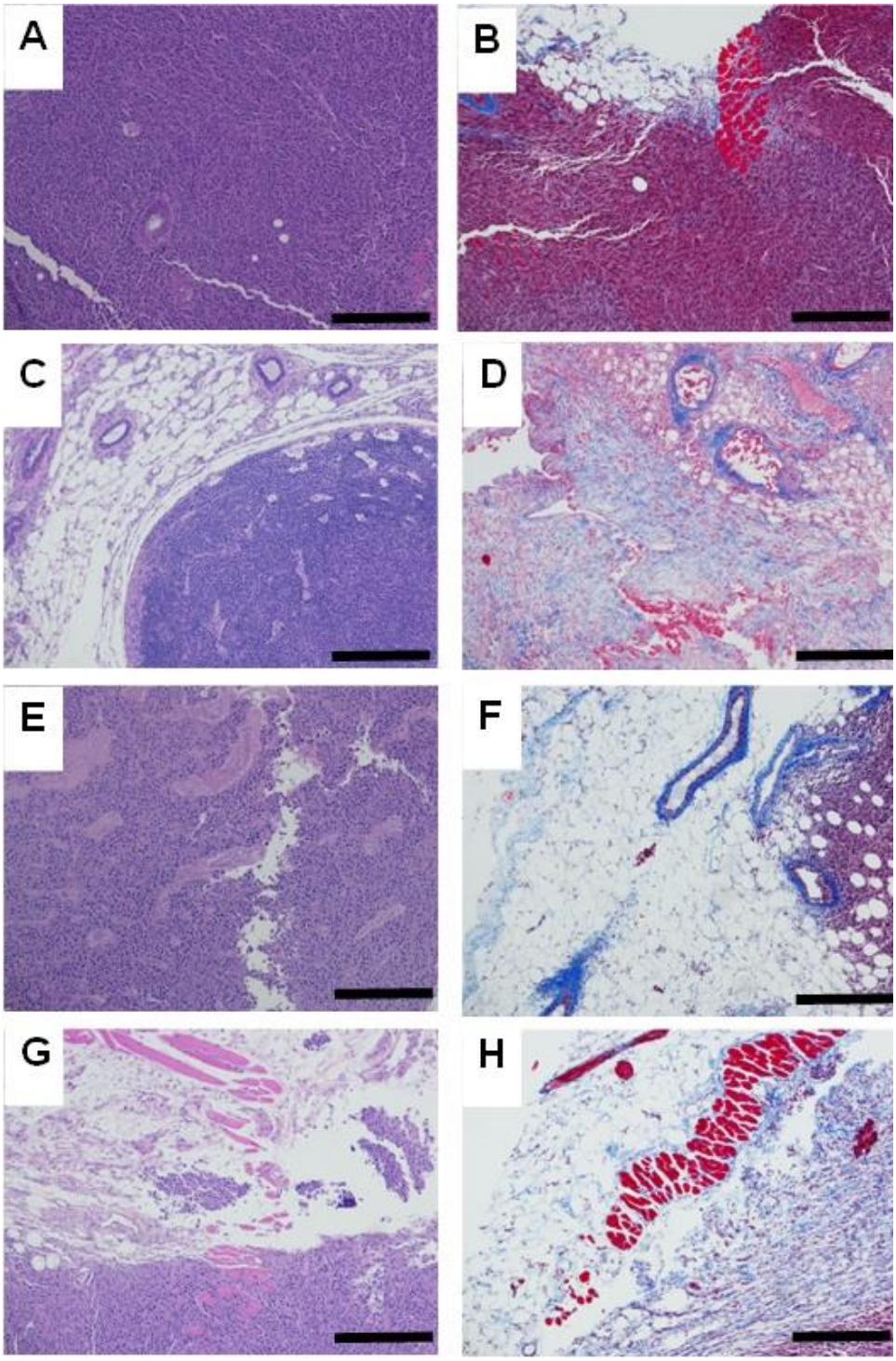

Figure 7. Histopathological H&E and Masson's Trichrome images in response to immune-checkpoint inhibitors. Image **(A,B)** from the control group IgG, image **(C,D)** from the PD-L1 group, image **(E,F)** from the CTLA-4 group, and image **(G,H)** from the COMB group. The scale bars represent 250 µm.

Table 1. Classification of ICI treatment. The results for leave-one-mouse-out random forest classification are shown for the prediction of–different ICI treated.

		True Labels			
		IgG	PD-L1	CTLA-4	COMB
Predicted Labels	IgG	7/8	0/9	0/9	1/8
	PD-L1	1/8	7/9	1/9	3/8
	CTLA-4	0/8	0/9	6/9	1/8
	COMB	0/8	2/9	2/9	3/8

Appendix A: IACUC Protocol Approval #20025

UNIVERSITY OF ARKANSAS

Office of Research Compliance

To:	Narasimhan Rajaram
Fr:	Jeff Wolchok
Date:	September 17th, 2019
Subject:	IACUC Approval
Expiration Date:	September 13th, 2021

The Institutional Animal Care and Use Committee (IACUC) has APPROVED your protocol # **20025:** *Optical spectroscopy of tumor response to immunotherapy*.

In granting its approval, the IACUC has approved only the information provided. Should there be any further changes to the protocol during the research, please notify the IACUC in writing (via the Modification form) prior to initiating the changes. If the study period is expected to extend beyond September 13th, 2021 you can submit a modification to extend project up to 3 years, or submit a new protocol. By policy the IACUC cannot approve a study for more than 3 years at a time.

The following individuals are approved to work on this study: Narasimhan Rajaram, Sina Dadgar, and Joel Rodriguez Tron. Please submit personnel additions to this protocol via the modification form prior to their start of work.

The IACUC appreciates your cooperation in complying with University and Federal guidelines involving animal subjects.

JCW/tmp

Appendix B: IACUC Protocol Approval #18066

UNIVERSITY OF ARKANSAS

Office of Research Compliance

To: Narasimhan Rajaram
FR: Craig Coon
Date: February 26th, 2018
Subject: IACUC Approval
Expiration Date: December 19th, 2018

The Institutional Animal Care and Use Committee (IACUC) has APPROVED your Modification to protocol # 18066 *Optical spectroscopy of tumor response to immunotherapy* add Sina Dadgar, Paola Monterroso-Diaz, and Joel Troncoso.

In granting its approval, the IACUC has approved only the information provided. Should there be any further changes to the protocol during the research, please notify the IACUC in writing (via the Modification form) prior to initiating the changes. If the study period is expected to extend beyond December 19th, 2018 you can submit a modification to extend project up to 3 years, or submit a new protocol. By policy the IACUC cannot approve a study for more than 3 years at a time.

The IACUC appreciates your cooperation in complying with University and Federal guidelines involving animal subjects.

CNC/tmp

Appendix C: List of published papers

1. Paidi S, **Troncoso JR**, Raj P, Diaz PM, Ivers J, Lee D, Avaritt N, Gies A, Quick C, Byrum S, Tackett A, Rajaram N, Barman I, *Raman spectroscopy and machine learning reveals early tumor microenvironmental changes induced by immunotherapy. Cancer Research*, 81(22): 5745-55, 2021

2. **Troncoso JR,** Diaz PM, Lee D, Quick C, Rajaram N, *Longitudinal monitoring of tumor response to immune checkpoint inhibitors using noninvasive diffuse reflectance spectroscopy*. Biomedical optics express 12(7):3982, 2021.

3. Vohra N, Chavez Esparza T, **Rodriguez Troncoso JI**, Rajaram N, Wu J, Coan PN, Jackson T, Bailey K, and El-Shenawee M *Mammary Tumors in Sprague Dawley Rats Induced by ENU for Evaluating Terahertz Imaging of Breast Cancer*. Journal of Medical Imaging 8(2): 023504, 2021

4. Dadgar S, **Rodriguez Troncoso JI**, Siegel ER, Curry NM, Griffin RJ, Dings PM, and Rajaram N. *Spectroscopic investigation of radiation-induced reoxygenation in radiation-resistant tumors*. Neoplasia 23(1):49-57, 2021

5. Dadgar S, **Rodriguez Troncoso JI**, and Rajaram N. *Optical spectroscopic sensing of tumor hypoxia.* Journal of Biomedical Optics 23(6): 067001, 2018.